DEM–CFD modeling and simulations of hydrodynamic characteristics and flow resistance coefficient in fixed-bed reactors

Yaping Li, Le Xie*, Yonghua Zhou, Chongwen Jiang, Hong Zhong,

College of Chemistry and Chemical Engineering, Central South University, Changsha 410083, China

* Correspondence to:

L. Xie E-mail: xiele2018@csu.edu.cn

Tel: +86- 731 88879616; Fax: +86 -731 88879616

Abstract

The ability to predict void fraction, pressure drop, and flow resistance coefficient in fixed-bed reactors is significant to their optimal design. In this study, the discrete element method (DEM) is combined with computational fluid dynamics (CFD) to simulate the hydrodynamic characteristics of fixed-beds. A realistic random packing structure for fixed-beds with spherical particles was generated via the DEM method and then meshed using Ansys ICEM software for the CFD simulation. A grid independency study was performed to select appropriate grid model parameters. A large set of numerical experiments was conducted to investigate the hydrodynamic characteristics with respect to different inlet velocities and particle sizes, and the simulated pressure drop data were used to calculate the flow resistance coefficient. The output flow resistance coefficients agreed well with those calculated by the classical models in laminar and turbulent flow regimes, thereby indicating the accuracy and advantage of the proposed DEM–CFD approach.

Introduction

Fixed-bed reactors have a wide range of applications in industrial practice including oil refining, catalytic cracking, and wastewater treatment.[1–5] In fixed-bed reactors, fluid passes through solid bodies (i.e., catalyst and packing material) that usually accompany complicated flow structures, which play a significant role in determining the heat and mass transfer performance. Therefore, many research studies have been focused on investigating the hydrodynamic characteristics of fixed-bed reactors to optimize its design.[6–10]

Owing to the inherent complicated packing structure, the design of fixed-bed reactors is mainly dependent on a homogeneous model over a long period of time. Many empirical correlations have been proposed to predict the void fraction and pressure drop.[11–13] However, empirical correlations cannot be applied in conditions involving low tube-to-particle diameter ratios due to the increased wall effect. With the development of experimental measurement techniques, the flow patterns in the porous media region can be visualized. The most common experimental techniques include particle image velocimetry (PIV),[14,15] magnetic resonance imaging (MRI),[16,17] and laser Doppler anemometry (LDA).[18,19] The detailed flow structures in fixed-bed reactors at different Reynolds numbers have been reported. However, there are certain applicable conditions for these measurement techniques. For example, MRI techniques can only be used for conditions involving nonmagnetic porous media.

In recent decades, computational fluid dynamics (CFD) modeling and simulation have been widely used to investigate flow field information in fixed-bed reactors

owing to the fast development of advanced numerical algorithms and computer technology. Using the CFD method, the fluid flow characteristics in the interstices between the particles can also be visualized. However, accurate simulation results are usually highly dependent on the 3D pore structure of porous media regions with high spatial resolution. Typically, there are two techniques to reconstruct the 3D pore structure: the experimental techniques (i.e., magnetic resonance imaging and X-ray computational tomography imaging) and discrete element method (DEM).[20–22] Advanced experimental techniques are capable of capturing detailed pore structures despite their inherent complexity. Conversely, DEM exhibits significant advantages in generating a packing structure characterized by random particles.[23–25] Furthermore, DEM combined with a CFD preprocessor (i.e., Ansys ICEM) is a powerful tool for meshing porous media regions. However, it is extremely challenging to mesh a packing structure with particle–particle and wall–particle contact points where the cells are extremely skewed, and this in turn can lead to convergence problems. To address this, Dixon et al. [26–29] conducted several studies and proposed many valuable mesh development methods. Additionally, significant research has been focused on modeling packing structures characterized by random nonspherical objects.[29-32] Yu et al.[33–35] reviewed the theoretical developments, applications, and inherent difficulties of these methods.

Based on the DEM–CFD method, the hydrodynamic characteristics of fixed-bed reactors have been widely investigated in recent years. Previous studies have focused on flow structures, pressure drop, and drag coefficient for a single-phase flow in

fixed-bed reactors. It was determined that the accuracy of the CFD results is highly dependent on the number of particles present.[36–38] Additionally, the influence of wall effects on the pressure drop cannot be neglected for low tube-to-particle diameter ratios.[39,40] Thus, the particle shape and size distribution play an important role in determining the performance of fixed-bed reactors. Based on these important research findings, the heat and mass transfer performance of fixed-bed reactors were also analyzed.[41,42] Generally, fixed-bed reactors exhibit unique hydrodynamic characteristics at different flow regimes. Therefore, the fixed-bed reactor should be investigated over a wide range of Reynolds numbers, which include creeping, transition, and turbulent regimes to gain a comprehensive and profound understanding of hydrodynamic characteristics.

The aim of this study involves numerically investigating the hydrodynamic characteristics of a fixed-bed reactor via DEM–CFD modeling and a simulation method. The packing structure of spherical particles of different sizes was developed using the DEM method and meshed via Ansys ICEM. Then, CFD simulations were performed to predict the void fraction, velocity, pressure drop, and flow resistance coefficient in fixed-bed reactors over a wide range of Reynolds numbers by adjusting the particle size and inlet velocity. The proposed DEM–CFD approach is validated by comparing the CFD results with those derived by empirical correlations in terms of the flow resistance coefficient. A large set of numerical experiment data are obtained and employed to analyze the hydrodynamic characteristics of fixed-bed reactors and interpret the deviations among the reported empirical correlations.

Correlations of flow resistance coefficient in fixed-bed reactors

In fixed-bed reactors, packed solid particles impede fluid flow. The flow resistance is mainly due to frictional loss and inertia, and it is manifested as a pressure drop in the macroscopic view. For a fixed-bed reactor, the pressure drop (Δp) is related to the flow velocity (v_0), fluid density (ρ_f), particle size (d_s), and bed porosity (α). The well-known pressure drop calculation correlation is defined as follows:

$$\Delta p = f \frac{L_r v_0^2 \rho_f (1-\alpha)}{d_s \alpha^3}$$

(1)

In **Eq. (1)**, the pressure drop is usually obtained via experimental measurement and numerical simulation. Then, the flow resistance coefficient (f) can be calculated. Over the past few decades, many research studies have been focused on the pressure drop characteristics at different fluid flow regimes. Many flow resistance coefficient correlations, which are typically a function of Reynolds number (Re), were proposed based on the experimental findings. The well-known Ergun resistance coefficient is defined as follows:[13]

$$f = \frac{150}{Re_\alpha} + 1.75$$

(2)

where the particle Reynolds number (Re_α) is defined as follows:

$$Re_\alpha = \frac{\rho_f d_s v_0}{\mu_f} \frac{1}{1-\alpha}$$

(3)

It should be noted that the resistance coefficient proposed by Ergun can be only valid in the viscous regime because the measured pressure drop data are in the range of $1<Re_\alpha<2400$. Some researchers indicated that the Ergun equation overpredicts the pressure drop for $Re_\alpha>700$. Therefore, a range of flow resistance coefficient correlations, with various forms of spherical and non-spherical particles, were proposed for different fluid flow regimes.

Schiller and Naumann[43] reported the fluid–solid resistance coefficient as follows:

$$f = \frac{24}{Re_\alpha}(1 + 0.15\,Re_\alpha^{0.687}) \qquad Re_\alpha < 800$$

(4)

Eq. (7) was adopted in the classical Gidaspow drag model.[44] Carman[45] proposed a flow resistance coefficient correlation for spherical particles by ignoring the wall effect as follows:

$$f = \frac{180}{Re_\alpha} + \frac{2.87}{Re_\alpha^{0.1}} \qquad 0.1< Re_\alpha < 60000$$

(5)

Dallavalle[46] defined the flow resistance coefficient as follows:

$$f = (0.63 + \frac{4.8}{Re_\alpha^{0.5}})^2$$

(6)

Hicks[8] also proposed a flow resistance coefficient correlation for spherical particles in the range of $300<Re_\varepsilon<60000$:

$$f = \frac{6.8}{\text{Re}_\alpha^{0.2}}$$
(7)

Similarly, Brauer[47] determined a relation by referring to the Carman equation. These two correlations are in exactly the same form but with different parameters.

$$f = \frac{160}{\text{Re}_\alpha} + \frac{3.1}{\text{Re}_\alpha^{0.1}} \qquad 0.01 < \text{Re}_\alpha < 40000$$
(8)

van Dijk and Wilms[48] proposed a flow resistance coefficient relationship based on the Carman–Kozeny correlation. Furthermore, they validated this correlation in the transitional flow regime.

$$f = \frac{130}{\text{Re}_\alpha^{0.8}} \qquad 5 < \text{Re}_\alpha < 100$$
(9)

As shown in the equation, the flow resistance coefficient exhibits various forms. Typically, there are two main factors that determine the flow resistance coefficient: the fluid flow regime and particle properties. The flow resistance coefficients exhibit significant differences in laminar flow, transitional flow, and complete turbulent flow regimes. The effects of particle properties are mainly evident in particle size and distribution, shape, roughness, and packing arrangement. As mentioned above, a large set of experiments have been conducted to investigate the hydrodynamic characteristics of fixed-bed reactors. However, the quantitative relationship between flow resistance and influencing factors is still not very clear. Therefore, a further study on the flow resistance coefficient in fixed-bed reactors is required.

DEM modeling, grid generation, and CFD simulation

The fixed-bed reactor (D = 60 mm and H = 120 mm) was randomly filled with spherical particles of different sizes. In this study, these packing structures were developed using the commercial DEM software. With respect to DEM modeling, spherical particles are generated at a specific height and are allowed to naturally fall under the action of gravity to simulate the real particle filling process. The physical parameters of granular material (i.e., density, shear modulus, and Poisson's ratio) and the contact parameters (i.e., friction coefficient and collision restitution coefficient) are set in the DEM to ensure an practical filling process. Additionally, a plane is used to slightly flatten the particles for simulating the process of particle compaction in the experimental process. Spherical particles with particle sizes corresponding to 4 mm, 6 mm, 8 mm, and 10 mm were used to fill the fixed-bed (see **Figure 1**). The filling height was 60 mm, and the number of filled particles varied. The packed structure parameters for each fixed bed are listed in **Table 1.** To minimize boundary effects and backflow, an empty bed of 30 mm was added at the fixed-bed inlet and outlet.

Then, the 3D packed models are exported in STL format using the user-defined Python program. The model files were imported into the commercial CFD preprocessor ICEM to generate mesh files for the CFD simulation, and an O-type segmentation method is adopted. Tetrahedral elements are used to generate unstructured mesh in the porous media region, and a hexahedral mesh is used for the empty pipe at both ends. Then, the two parts of the mesh model are assembled, and the interface boundary conditions are used to transfer data between regions. The mesh size can be characterized by the side length of the grid element. In this study, the

maximum mesh element of the unstructured grid is 0.4 mm and that of the structural grid is 0.8 mm.
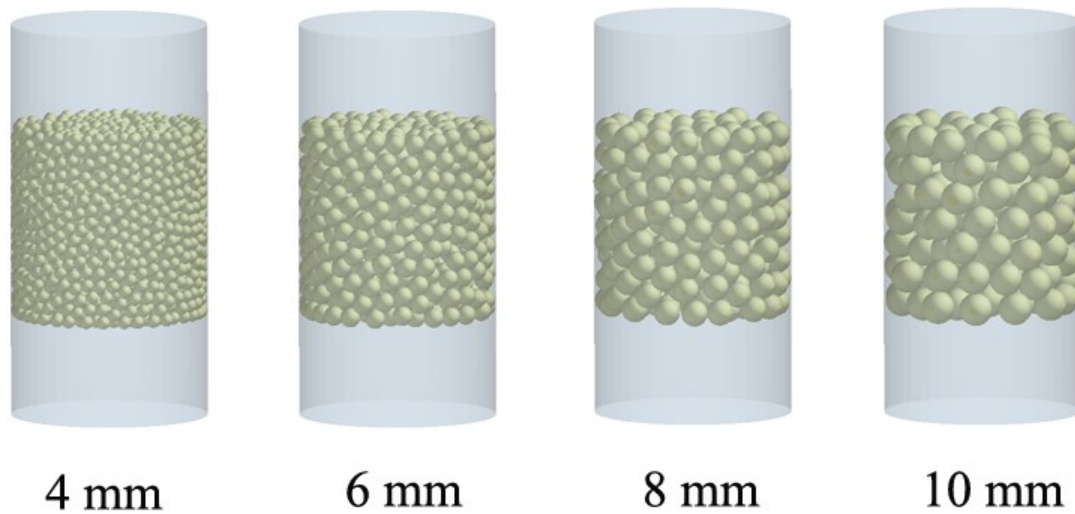

Figure 1. The packed structure model for fixed-bed filled with spherical particles with particle sizes of 4 mm, 6 mm, 8 mm, and 10 mm, respectively

Table 1 The packed structure parameters for each fixed-bed reactor

Structure parameters for fixed-bed	Particle size (mm)	Particle numbers	Voidage (True value)	Voidage (Volume average)
Pipe diameter:	4	3000	0.4445	0.4477
60 mm	6	865	0.4594	0.4621
Packing height	8	363	0.4623	0.4632
60 mm	10	180	0.4792	0.4796

Based on the developed mesh model, CFD simulations can be conducted to predict the hydrodynamic characteristics in fixed-bed reactors. The velocity and pressure fields are calculated by solving the continuity equation, momentum equation, and turbulent model. Subsequently, the obtained pressure drop can be employed to calculate the flow resistance coefficient.

In this study, a single-phase flow system (air, ρ = 1.225 kg/m^3, μ = 1.7894 $\times10^{-5}$

Pa•s) was chosen to investigate the effects of the flow rate and particle size on the pressure drop in a laboratory-scale fixed-bed reactor. The air entered from the bottom of the reactor at a uniform velocity and was discharged from the top of the reactor at constant pressure. The flow resistance coefficient correlation was determined based on a large set of numerical simulation experiments. The output pressure drop and drag coefficient were compared with those derived from classical empirical correlations, as mentioned above. The detailed CFD model equations are as follows:

Continuity equation:

$$\frac{\partial}{\partial t}(\rho) + \nabla \cdot (\rho \vec{v}) = 0$$

(10)

Momentum equation:

$$\frac{\partial}{\partial t}(\rho \vec{v}) + \nabla \cdot (\rho \vec{v} \vec{v}) = -\nabla p + \nabla \cdot \overline{\overline{\tau}}$$

(11)

$$\overline{\overline{\tau}} = (\mu + \mu_t)[(\nabla \vec{v} + \nabla \vec{v}^T) - \frac{2}{3}\nabla \vec{v} I]$$

(12)

where p denotes pressure, $\overline{\overline{\tau}}$ denotes stress tensor, μ denotes molecular viscosity, and

μ_t denotes eddy viscosity, which is computed by combining k and ε as follows:

k–ε turbulent model

$$\frac{\partial}{\partial t}(\rho k) + \nabla \cdot (\rho k \vec{v}) = \nabla \cdot (\mu + \frac{\mu_t}{\sigma_k} \nabla k) + G_k - \rho \varepsilon \qquad (13)$$

$$\frac{\partial}{\partial t}(\rho \varepsilon) + \nabla \cdot (\rho \varepsilon \vec{v}) = \nabla \cdot (\mu + \frac{\mu_t}{\sigma_\varepsilon} \nabla \varepsilon) + \frac{\varepsilon}{k}(C_{1\varepsilon} G_k - C_{2\varepsilon} \rho \varepsilon) \qquad (14)$$

where

$$\mu_t = \rho C_\mu \frac{k^2}{\varepsilon} \qquad (15)$$

The model constants: $C_\mu = 0.09$, $\sigma_k = 1.0$, $\sigma_\varepsilon = 1.3$, $C_{1\varepsilon} = 1.44$, $C_{2\varepsilon} = 1.92$.

Results and discussion

Grid independency study

With respect to the 3D geometric model constructed using the particles, the grid resolution has an important effect on the void fraction of the packed bed, and this in turn determines the predicted pressure drop. Therefore, grid independency analysis should be performed before the CFD simulation. The true void fraction of the packed bed can be calculated based on the physical modeling via the DEM method. Furthermore, the volume of voids in the packed bed is equal to that of the flow region, which can be calculated using Ansys Fluent. In this study, the appropriate mesh precision is selected based on the comparison of the void fraction calculated via DEM and CFD methods. **Figure 2** shows the voidage distribution in the axial of a fixed-bed packed with spherical particles of different sizes. The detailed packed structure parameters are listed in **Table 1**. As shown, the voidage increases as particle size increases in the same fixed-bed reactor. For each fixed-bed reactor, the porous media

region is meshed with different grid model parameters (maximum grid size). For example, when the fixed-bed reactor was packed with 4 mm spherical particles, the total number of particles was 3000 and the true voidage was 44.45 %. When the maximum grid size was 1.0 mm, the predicted voidage was approximately 50 %, which is significantly higher than the true voidage value. With the improvement in mesh accuracy, the predicted voidage is increasingly closer to its true value. As shown, when the maximum grid size is less than 0.4 mm, i.e., one tenth of the particle size, the voidage does not vary with respect to grid size, and the predicted average volume of voidage is 44.77 %. In this study, the mesh accuracy with a maximum grid size of 0.4 mm was chosen in the following CFD simulations to determine the mean between the computing cost and simulation accuracy.

Additionally, the packed structures of the fixed-bed reactor differ even though the same reactor structure, number of particles, and particle size are used. This is because the packed process is random. **Figure 3** shows the packed structure of a fixed-bed reactor filled with 6 mm particles through multiple filling. The detailed voidage distribution in the axial of the packed fixed-bed is listed in **Table 2**. Although the local voidage can vary, the average volume of the voidage in the fixed-bed almost remains constant, and the absolute deviation is less than 0.07 %.

In summary, the developed mesh models are appropriate because the predicted voidages are in good agreement with the true values. A further CFD simulation is conducted based on these mesh models.
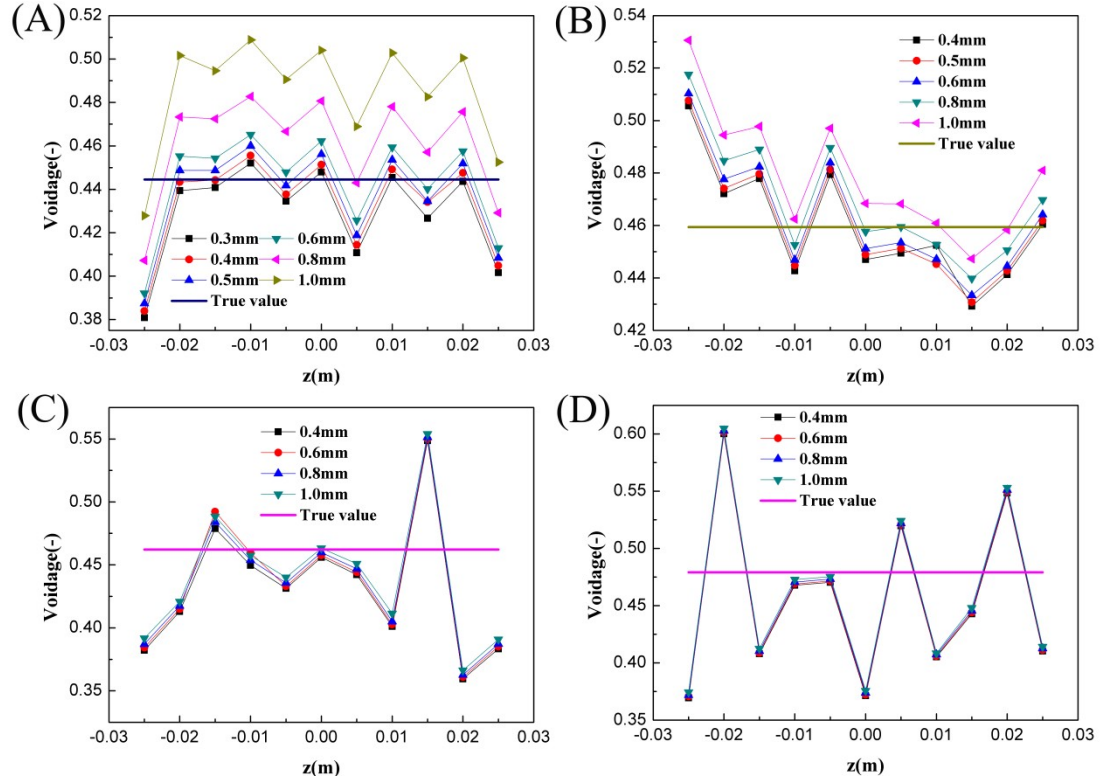
Figure 2. The voidage distribution in the axial of fixed-bed packed with spherical particles of different sizes.

Table 2. The local voidage in fixed-bed reactor packed with 6 mm particle size

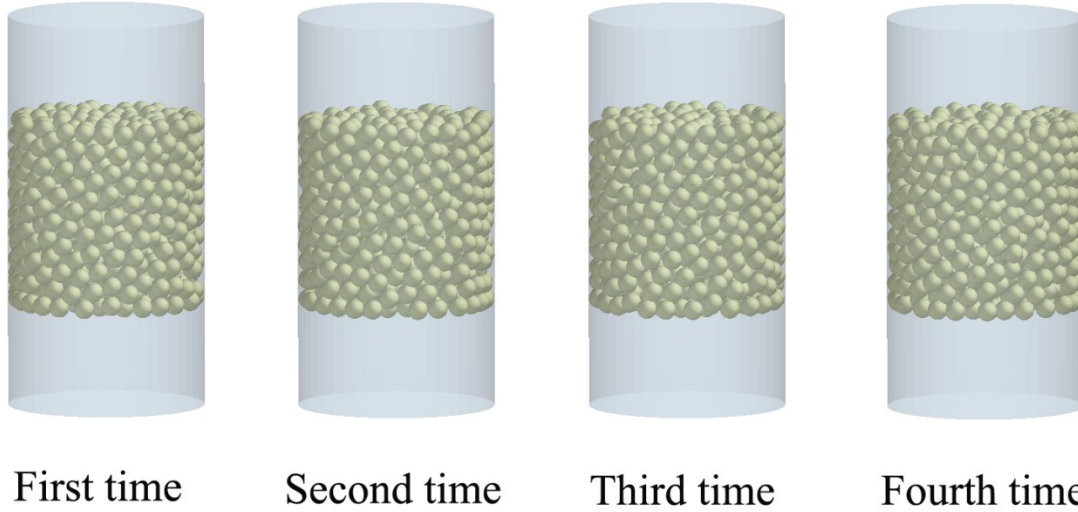| z(m)	First time	Second time	Third time	Fourth time
-0.025	0.5056	0.4530	0.4528	0.4454
-0.02	0.4721	0.4366	0.4405	0.4478
-0.015	0.4779	0.4544	0.4551	0.4763
-0.01	0.4427	0.4842	0.4699	0.4782
-0.005	0.4794	0.4856	0.5132	0.4945
0	0.4471	0.4146	0.4288	0.4445
0.005	0.4495	0.4506	0.4340	0.4472
0.01	0.4524	0.4349	0.4267	0.4382
0.015	0.4293	0.4530	0.4708	0.4522
0.02	0.4413	0.4432	0.4655	0.4495
0.025	0.4605	0.4583	0.4788	0.4536
Volume average	0.4621	0.4614	0.4615	0.4616

Figure 3. The packed structure of fixed-bed through multiple filling when the particle size is 6 mm

Hydrodynamic characteristics

Based on the developed 3D mesh model and CFD model, the hydrodynamic characteristics of fixed-bed reactors with different packing structures are investigated. It is known that pressure drop is one of the most important performance evaluation parameters for fixed-bed reactors. As discussed above, the pressure drop exhibits unique characteristics in different flow regimes.

In this study, the pressure profiles were simulated over the inlet flow rate range of 0.001–3 m/s and a tube-to-particle diameter ratio in the range of 6–15, where particle Reynolds number (Re_α) is in the range of 0.5–4000. The pressure drop, termed as the difference in the average pressure values at the inlet and outlet and velocity field are obtained and employed to analyze the hydrodynamic characteristics of fixed-bed reactors.

Fig. 4 shows the simulated pressure drop as a function of the air inlet velocity with respect to varying particle sizes. Additionally, the least squares method was employed to fit the simulated data. The pressure drop corresponds to zero when the air inlet velocity is zero. Based on the form of the Eugen equation—the parabolic equation without an intercept—an equation of the form $\Delta p = av^2 + bv$, is used as the target fitting function in this study. As shown in **Fig. 4**, there is a typical quadratic function relationship between the pressure drop and air inlet velocity ($R^2 > 0.99$). As discussed by Niven,[49] the local pressure losses, such as expansion and contraction, often manifest as v^2 pressure loss. These effects also occur in the laminar flow regime. However, they have a limited effect on the pressure drop due to the low velocity. Typically, the local losses, also known as inertia losses, are dominant in the fully turbulent flow regime. The relationship between the pressure drop and low inlet air velocity (<0.025 m/s), with the corresponding Re_r in the range of 0.5–30, is shown in **Figure 5**. As shown, the pressure drops values exhibit completely different characteristics in the laminar flow regime when compared to those in the turbulent flow regime. A linear relationship between and inlet velocity ($R^2 > 0.99$) was observed in the laminar flow regime, thereby indicating that frictional losses were dominant. The observed linear or quadratic dependency between the pressure drop and velocity is in good agreement with the classical Ergun equation, thereby validating the proposed DEM–CFD model.

The effect of particle size on the pressure drop is also shown in **Figures 4** and **5**. The pressure drop is sensitive to the particle size. As mentioned above, the voidage increases from 44.77 % to 47.96 % when the particle size decreases from 10 mm to 4 mm. The decreased voidage is the main reason for the increase in pressure drop. **Figure 6** shows the contours of static pressure values in fixed-bed reactors when the air inlet velocity is 1 m/s. The pressure profile is almost linear along the bed height. However, local pressure can fluctuate due to changes in the channel diameter. Therefore, the linear scaling of the pressure drop is typically used for the actual packed bed reactor. Additionally, constant pressures are observed at the inlet and outlet sections, thereby indicating that the entrance and exit effects are negligible.

Furthermore, the velocity contour and velocity vector were obtained to investigate the hydrodynamic performance of the fixed-bed reactor. **Figure 7** shows the distribution of velocity at $z = 0$ plane when the inlet air velocity is 1 m/s. Given that the volume average voidage is 0.4796, the average velocity in the bed is 2.1 m/s. As shown in **Figure 7**, the average velocity of the facet is about 3.1 m/s. This velocity, which is higher than the average velocity, is due to the uneven distribution of local voidage. Moreover, the change in the flow channel diameter leads to a change in velocity. The distribution characteristics of velocity magnitude can also be reflected by the iso-surface velocities (i.e., 3 m/s and 5 m/s). Although the average velocity is 3.1 m/s, a higher velocity, such as 5 m/s, occupies an important position over the entire velocity distribution. From the velocity vector in **Figure 7**, there are many vortexes in the interstices between particles and between particles and the wall. These

flow characteristics are determined by the complicated packing structures, which play

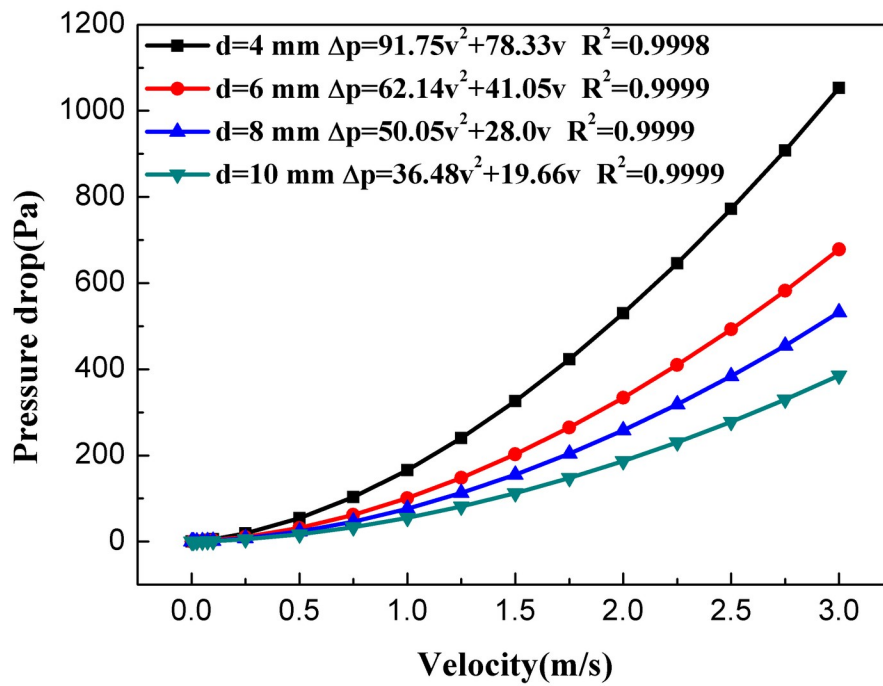a significant role in affecting the heat and mass transfer performance of fixed-bed

reactors.

Figure 4 The simulated pressure drop as a function of the air inlet velocity with
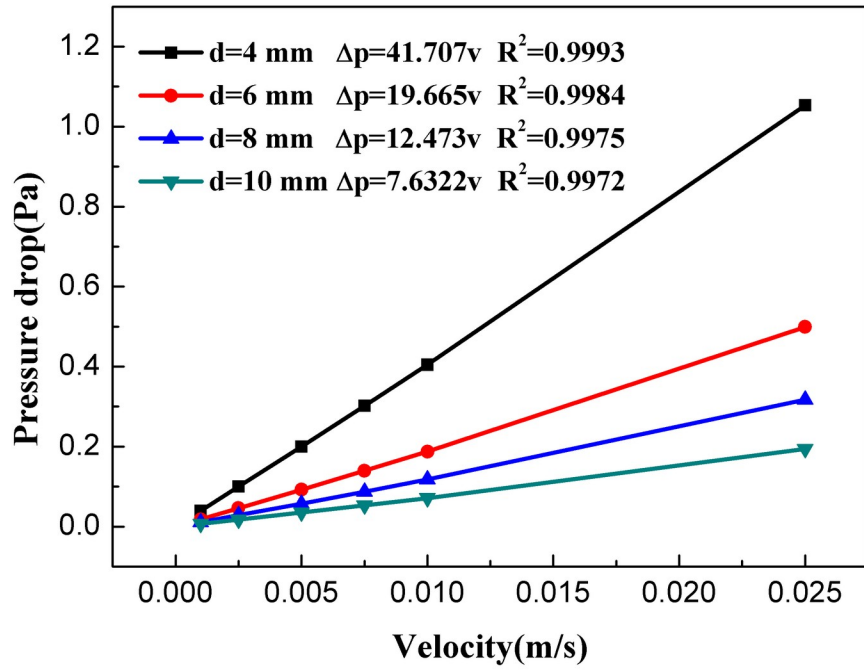
varying particle size.

Figure 5. The relationship between pressure drop and low air inlet velocity (<0.025m/

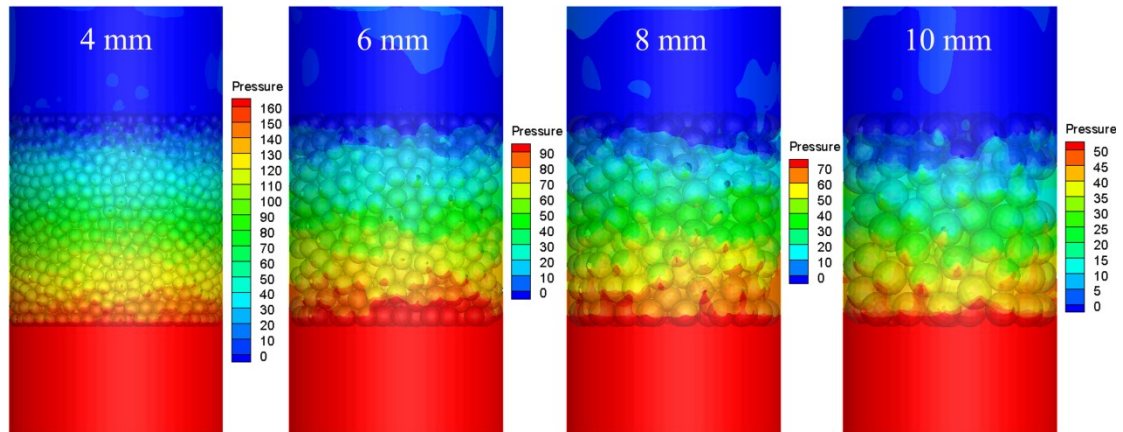s), with the corresponding Re_α in the range of 0.5-30

Figure 6. The contours of static pressures in fixed-bed reactors when the air inlet
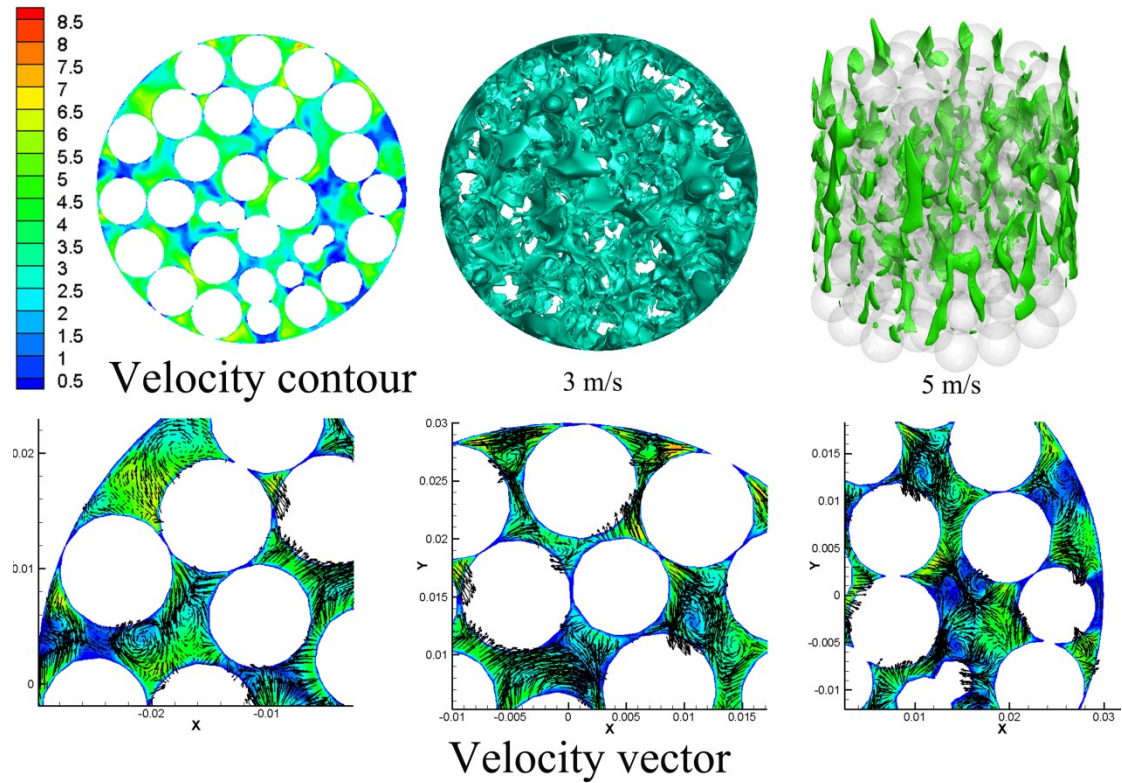
velocity is 1 m/s

Figure 7. The velocity contour and velocity vector at z=0 plane when the air inlet

velocity is 1 m/s

Flow resistance coefficient correlations

In this study, 84 pressure drop datasets at different particle sizes and air inlet

velocities were obtained and used to extrapolate the flow resistance coefficient

correlation. **Figure 8** displays the relationship between the resistance coefficient and

Re_α in a fixed-bed reactor with respect to different particle sizes. It should be noted

that the calculated flow resistance coefficients are based on to the magnitude of Re_α.

Generally, the flow resistance coefficient is high at a low Reynolds number, and the

converse holds as well. As shown, the flow resistance coefficients appear to share the

same trend in the low Reynolds number range, and the particle size has a limited

effect on the flow resistance coefficient. However, in the high Reynolds number

range, the effect of particle size on the resistance coefficient is clear. The small

particles usually exhibit low resistance coefficient values at the same Reynolds number.

Additionally, all the extrapolated resistance coefficients were compared with those calculated by the classical models (see **Figure 9**). To show the comparison results more clearly, the flow resistance coefficients are shown with respect to the magnitude of Re_α. In the low Reynolds number range, the calculated flow resistance coefficients are in good agreement with most of the reported correlations, such as Carman, Ergun, Brauer, and Dijk–Wilms correlation. However, the Schiller–Naumann, Dallavalle, and Hicks correlation appear to be inadequate. Hicks[8] indicated that their flow resistance coefficient correlation should be used in the range of $300<Re_\alpha<60000$. Therefore, the scope of application of the Schiller–Naumann and Dallavalle correlations should be clearly stated.

Figure 9B shows the comparison results of the flow resistance coefficient in the high Reynolds number range. The predictions by Schiller–Naumann and Dallavalle correlations are still lower than those obtained in this study. For the Dijk–Wilms correlation, it is only valid in the range of $5<Re_\alpha<100$. As mentioned above, our data is in good agreement with the Dijk–Wilms correlation in the range $0.5<Re_\alpha<50$. However, the underestimated flow resistance coefficients by the Dijk–Wilms correlation are also observed in the high Reynolds number range. Conversely, Hicks correlation exhibits poor predictive performance in the range $0.5<Re_\alpha<50$. However, it exhibits good predictive performance in the range of $500<Re_\alpha<4000$.

Additionally, the Ergun correlation overestimates the flow resistance coefficients

at high Reynolds numbers. This is due to the fact that the Ergun correlation was proposed by the measured pressure drop data in the viscous regime. Many researchers have observed the overestimated pressure drop by the Ergun correlation at higher Reynolds numbers. [7,9]

As stated above, the flow resistance coefficients obtained in this study are in good agreement with those calculated by the classical models in laminar and turbulent flow regimes. The comparison results indicate that the proposed DEM–CFD method is effective. The inherent deviation in the existing correlations can be due to the limited experimental data, which cannot cover the entire flow regime. Furthermore, the particle size distribution and particle shape can significantly affect the pressure drop in the actual process of the experiments. These factors are not considered in this study, and they will be closely examined in future studies. However, the parameters in the flow resistance coefficient correlation must be used judiciously to improve the prediction accuracy of the pressure drop and resistance coefficient.
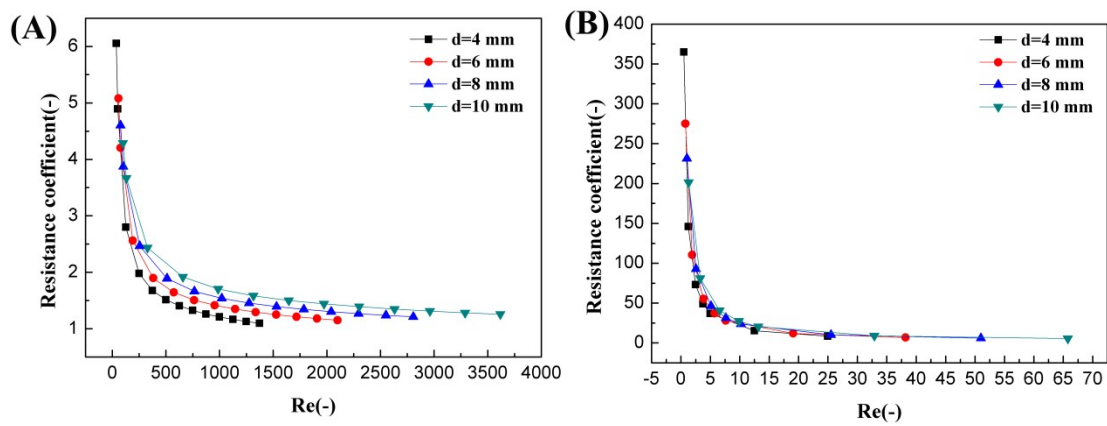

Figure 8. The relationship between resistance coefficient and Re_α in fixed-bed reactor under different particle sizes.
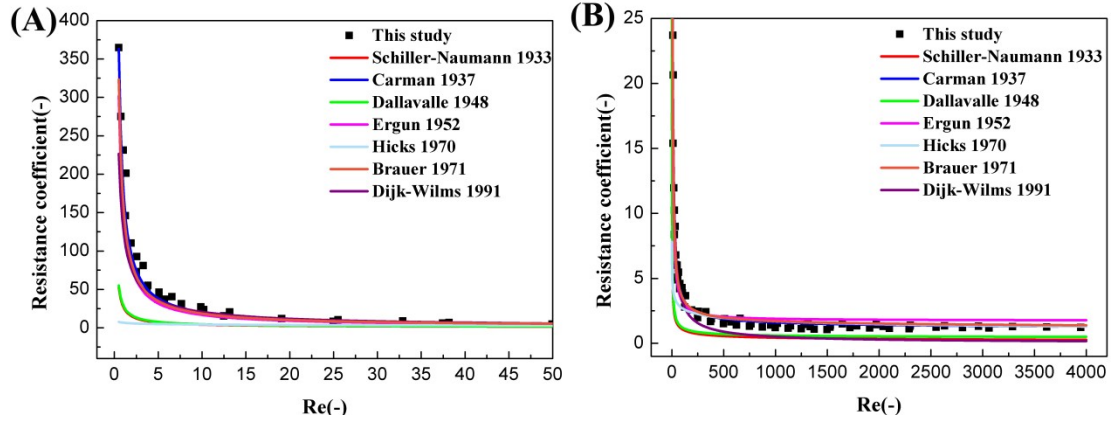
Figure 9. The comparison results of CFD results and classical correlations in terms of flow resistance coefficient under different Reynolds numbers

Conclusion

In this study, the DEM was combined with CFD to simulate the hydrodynamic characteristics of fixed-bed reactors with varying tube-to-particle diameter ratios. The realistic random packing structure for the fixed bed can be effectively developed by the DEM method because the predicted voidages were in good agreement with the true values. The effects of particle size and inlet velocity on the pressure drop were investigated via CFD simulation. A typical quadratic function relationship between the pressure drop and inlet velocity was observed within the entire flow regime. A linear relationship between the pressure drop and inlet velocity was also suitable in the laminar flow regime. Moreover, the pressure profile was almost linear along the bed height, and many vortexes were observed in the interstices between particles and between particles and the wall. The output flow resistance coefficients were in good agreement with those calculated via the classical models in laminar and turbulent flow regimes, thereby indicating the accuracy and advantage of the proposed DEM–CFD approach.

Acknowledgments

Notation

C_{1r}, C_{2r}, C_{μ} Turbulence model parameter, dimensionless

d_s Particle size, m

f Resistance coefficient, dimensionless

G_k Turbulence model parameter, dimensionless

I Unit tensor, dimensionless

k Turbulence kinetic energy, $m^2 \cdot s^{-2}$

L_r Length, m

p Pressure, Pa

Re Reynolds number, dimensionless

t Time, s

v Velocity, $m \cdot s^{-1}$

Greek letters

α Voidage, dimensionless

ρ Density, $kg \cdot m^{-3}$

$\bar{\bar{\tau}}$ Stress tensor, Pa

μ Viscosity, $Pa \cdot s$

ε Turbulence dissipation rate, s^{-1}

σ Turbulence model parameter, dimensionless

Literature Cited

1. Castillo-Araiza CO, López-Isunza F. Modeling the partial oxidation of o-xylene in an industrial packed bed catalytic reactor: The role of hydrodynamics and catalyst activity in the heat transport. *Ind. Eng. Chem. Res.* 2010;49:6845–6853.

2. Ranade VV. Computational flow modeling for chemical reactor engineering. *Academic Press*, New York, 2002.

3. Wehinger GD, Klippel F, Kraume M. Modeling pore processes for particle-resolved CFD simulations of catalytic fixed-bed reactors. *Comput. Chem. Eng*. 2017;101: 11-22.

4. Wehinger GD, Eppinger T, Kraume M. Detailed numerical simulations of catalytic fixed-bed reactors: Heterogeneous dry reforming of methane. *Chem. Eng. Sci.* 2015;122:197–209.

5. Wehinger GD, Kraume M, Berg V, Korup O, Mette K, Schlogl R, Behrens M, Horn R. Investigating dry reforming of methane with spatial reactor profiles and particle-resolved CFD simulations. *AIChE J.* 2016;62:4436–4452.

6. Tallmadge JA. Packed bed pressure drop-an extension to higher Reynolds numbers. *AIChE J.* 1970;16:1092-1093.

7. Allen KG, Von Backström TW, Kröger DG. Packed bed pressure drop dependence on particle shape, size distribution, packing arrangement and roughness. *Powder Technol.* 2013;246:590-600.

8. Hicks RE. Pressure drop in packed beds of spheres. *Indus. Eng. Chem. Fund.*

1970;9:500-502.

9. Bai H, Theuerkauf J, Gillis PA, Witt PM. A coupled DEM and CFD simulation of flow field and pressure drop in fixed bed reactor with randomly packed catalyst particles. *Indus. Eng. Chem. Res.* 2009;48:4060-4074.

10. Pavlišič A, Pohar A, Likozar B. Comparison of computational fluid dynamics (CFD) and pressure drop correlations in laminar flow regime for packed bed reactors and columns. *Powder Technol.* 2018;328:130-139.

11. Leva M, Grummer M. Pressure drop through packed tubes: Part III prediction of voids in packed tubes. *Chem. Eng. Prog.* 1947;43:713–718.

12. Dixon AG. Correlations for the wall and particle shape effects on fixed bed voidage. *Can. J. Chem. Eng.* 1988;66:705–708.

13. Ergun S. Fluid flow through packed columns, *Chem. Eng. Prog.* 1952;48:89-94.

14. Saleh S, Thovert JF, Adler PM. Flow along porous media by particle image velocimetry. *AIChE J.* 1993;39:1765–1773.

15. Beguin R, Philippe P, Faure Y.-H. Pore-scale flow measurements at the interface between a sandy layer and a model porous medium: application to statistical modeling of contact erosion. *J. Hydraul. Eng.* 2013;139:1–11.

16. Köhl MH, Lu G, Third JR, Häberlin M, Kasper L, Prüssmann KP, Müller CR. Magnetic resonance imaging (MRI) study of jet formation in packed beds. *Chem. Eng. Sci.* 2013;97:406–412.

17. Suekane T, Yokouchi Y, Hirai S. Inertial flow structures in simple packed bed of spheres. *AIChE J.* 2003;49:10–17.

18. Giese M, Rottschafer K, Vortmeyer D. Measured and modeled superficial flow

profiles in packed beds with liquid flow. *AIChE J.* 1998;44:484–490.

19. Calis HPA, Nijenhuis J, Paikert BC, Dautzenberg FM, van den Bleek CM. CFD modeling and experimental validation of pressure drop and flow profile in a novel structured catalytic reactor packing. *Chem. Eng. Sci.* 2001;56:1713–1720.

20. Baker MJ, Young PG, Tabor GR. Image based meshing of packed beds of cylinders at low aspect ratios using 3D MRI coupled with computational fluid dynamics. *Comput. Chem. Eng.* 2011;35:1969–1977.

21. Kurotori T, Zahasky C, Hejazi SAH, Shah SM, Benson SM, Pini R. Measuring, imaging and modelling solute transport in a microporous limestone. *Chem. Eng. Sci.* 2019;196:366-383.

22. Gunde AC, Bera B, Mitra SK. Investigation of water and CO_2 (carbon dioxide) flooding using micro-CT (micro-computed tomography) images of Berea sandstone core using finite element simulations. *Energy.* 2010;35:5209-5216.

23. Rong LW, Dong KJ, Yu AB. Lattice-Boltzmann simulation of fluid flow through packed beds of uniform spheres: Effect of porosity. *Chem. Eng. Sci.* 2013;99: 44–58.

24. Rong LW, Zhou ZY, Yu AB. Lattice-Boltzmann simulation of fluid flow through packed beds of uniform ellipsoids. *Powder Technol.* 2015;285:146–156.

25. Rong LW, Dong KJ, Yu AB. Lattice-Boltzmann simulation of fluid flow through packed beds of spheres: Effect of particle size distribution. *Chem. Eng. Sci.* 2014;116:508–523.

26. Dixon AG, Walls G, Stanness H, Nijemeisland M, Stitt EH. Experimental

validation of high Reynolds number CFD simulations of heat transfer in a pilotscale fixed bed tube. *Chem. Eng. J.* 2012;200–202:344–356.

27. Dixon AG, Nijemeisland M, Stitt EH. Systematic mesh development for 3D CFD simulation of fixed beds: Contact points study. *Comput. Chem. Eng.* 2013;48:135−153.

28. Dixon AG, Taskin ME, Nijemeisland M, Stitt HH. Systematic mesh development for 3D CFD simulation of fixed beds: Single sphere study. *Comput. Chem. Eng.* 2011;35:1171−1185.

29. Partopour B, Dixon AG. An integrated workflow for resolved-particle packed bed models with complex particle shapes. *Powder Technol.* 2017;322:258−272.

30. Moghaddam EM, Foumeny EA, Stankiewicz AI, Padding JT. Rigid body dynamics algorithm for modeling random packing structures of nonspherical and nonconvex pellets. *Indus. Eng. Chem. Res.* 2018;57:14988-15007.

31. Eppinger T, Seidler K, Kraume M. DEM-CFD simulations of fixed bed reactors with small tube to particle diameter ratios. *Chem. Eng. J.* 2011;166:324-331.

32. Lu G, Third JR, Müller CR. Discrete element models for non-spherical particle systems: From theoretical developments to applications. *Chem. Eng. Sci.* 2015;127:425−465.

33. Zhong W, Yu AB, Liu X, Tong Z, Zhang H. DEM/CFD-DEM Modelling of non-spherical particulate systems: Theoretical developments and applications. *Powder Technol.* 2016;302:108−152.

34. Zhu HP, Zhou ZY, Yang RY, Yu AB. Discrete particle simulation of particulate

systems: A review of major applications and findings. *Chem. Eng. Sci.* 2008;63: 5728–5770.

35. Zhu HP, Zhou ZY, Yang RY, Yu AB. Discrete particle simulation of particulate systems: Theoretical developments. *Chem. Eng. Sci.* 2007;62:3378–3396.

36. Nijemeisland M, Dixon AG. CFD study of fluid flow and wall heat transfer in a fixed bed of spheres. *AIChE J.* 2004;50:906–921.

37. Guardo A, Coussirat M, Larrayoz MA, Recasens F, Egusquiza E. Influence of the turbulence model in CFD modeling of wall-to-fluid heat transfer in packed beds. *Chem. Eng. Sci.* 2005;60:1733–1742.

38. Calis HPA, Nijenhuis J, Paikert BC, Dautzenberg FM, van den Bleek CM. CFD modeling and experimental validation of pressure drop and flow profile in a novel structured catalytic reactor packing. *Chem. Eng. Sci.* 2001;56:1713–1720.

39. Reddy RK, Joshi JB. CFD modeling of pressure drop and drag coefficient in fixed and expanded beds. *Chem. Eng. Res. Des.* 2008;86:444–453.

40. Reddy RK, Joshi JB. CFD modeling of pressure drop and drag coefficient in fixed beds: Wall effects. *Particuology.* 2010;8:37-43.

41. Dong Y, Sosna B, Korup O, Rosowski F, Horn R. Investigation of radial heat transfer in a fixed-bed reactor: CFD simulations and profile measurements. *Chem. Eng. J.* 2017;317:204-214.

42. Zhang M, Dong H, Geng Z. Computational study of flow and heat transfer in fixed beds with cylindrical particles for low tube to particle diameter ratios. *Chem. Eng. Res. Des.* 2018;132:149-161.

43. Schiller L, Naumann A. Über die grundlegenden berechnungen bei der

schwerkraftauf-bereitung. *Z. Ver. Dtsch. Ing.* 1933;*77:* 318-320.

44. Gidaspow D, Bezburuah R, Ding J. Hydrodynamics of circulating fluidized beds: kinetic theory approach. *Fluidization VII Proceedings of the 7th Engineering Foundation Conference on Fluidization*, 1992;75-82.

45. Carman PC. Fluid flow through granular beds. *Trans. Inst. Chem. Eng.* 1937;15: 32-48.

46. Dallavalle JM. Micromeritics: the technology of fine particles. *2nd ed. Pitman*, London. 1948.

47. Brauer H. Grundlagen der Einphasen –und Mehrphasenströmungen, Sauerländer AG, Aarau, 1971.

48. van Dijk JC, Wilms DA. Water treatment without waste material-fundamentals and state of the art of pellet softening. *J. Water Supply Res. Technol. AQUA*, 1991;*40:* 263-280.

49. Niven RK. Physical insight into the Ergun and Wen & Yu equations for fluid flow in packed and fluidized beds. *Chem. Eng. Sci.* 2002;57:527–534.